

See discussions, stats, and author profiles for this publication at: <https://www.researchgate.net/publication/233417771>

# Catalysis Kinetics and Porous Analysis of Rolling Activated Carbon-PTFE Air-Cathode in Microbial Fuel Cells

ARTICLE in ENVIRONMENTAL SCIENCE & TECHNOLOGY · NOVEMBER 2012

Impact Factor: 5.33 · DOI: 10.1021/es303619a · Source: PubMed

---

CITATIONS

59

---

READS

131

## 3 AUTHORS, INCLUDING:



Xin Wang

Nankai University

58 PUBLICATIONS 1,745 CITATIONS

[SEE PROFILE](#)

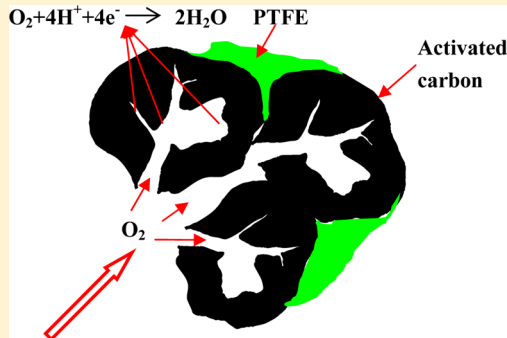
## Catalysis Kinetics and Porous Analysis of Rolling Activated Carbon-PTFE Air-Cathode in Microbial Fuel Cells

Heng Dong, Hongbing Yu,\* and Xin Wang\*

MOE Key Laboratory of Pollution Processes and Environmental Criteria/Tianjin Key Laboratory of Environmental Remediation and Pollution Control/Research Center for Cleaner Production/College of Environmental Science and Engineering, Nankai University, No. 94 Weijin Road, Nankai District, Tianjin 300071, China

 Supporting Information

**ABSTRACT:** The microbial fuel cell (MFC), being an environment-friendly technology for wastewater treatment, is limited by low efficiency and high cost. Power output based on capital cost had been greatly increased in our previous work by introducing a novel activated carbon (AC) air-cathode (ACAC). The catalysis behavior of this ACAC was studied here based on catalysis kinetics and pore analysis of both carbon powders and catalyst layers (CLs). Plain AC (AC1#), ultracapacitor AC (AC2#), and non-AC (XC-72) powders were used as catalysts. The electron transfer number (*n*) of oxygen reduction reaction (ORR) with CLs increased by 5–23% compared to those *n* values of corresponding carbon powders before being rolled to CLs with PTFE, while the *n* value of Pt/C decreased by 38% when it was brushed with Nafion as the CL, indicating that rolling procedure with PTFE binder substantially increased the catalytic activity of carbon catalysts. Two–four times larger in micropore area of AC powders than non-AC powder resulted in 1.3–1.9 times increase in power density of MFCs. In addition, more uniform distribution of microporosity was found in AC1# than in AC2#, which could be the reason for the 25% increase in power density of ACAC1# ( $1355 \pm 26 \text{ mW}\cdot\text{m}^{-2}$ ) compared to  $1086 \pm 8 \text{ mW}\cdot\text{m}^{-2}$  of ACAC2#.



### INTRODUCTION

Microbial fuel cells (MFCs) have been generally acknowledged as a promising “green” approach for wastewater treatment to retrofit the existing enormous power consumption infrastructure.<sup>1</sup> Microorganisms attaching on the anode function as regenerated biocatalysts to continuously convert biodegradable contaminants in wastewaters into a clean electrical energy. Oxygen has superiority as the oxidant for MFCs owing to its direct and inexhaustible availability together with positive redox potential and the harmless reduction product (water). As a stand-alone method for wastewater treatment in the future, the first economic benefit of MFCs is the avoidance of electrical power consumed for aeration.<sup>2</sup> Air-cathode MFC is such a device which provides fast passive transfer of oxygen to the cathodic reaction site using natural air-flow.<sup>3,4</sup> However, the inherent unideal conditions in MFCs involving ambient temperature as well as mostly neutral pH put thermodynamic and kinetic constraints to the efficiency of oxygen reduction reaction (ORR) on the cathode. This problem is much more serious when performed at unmodified electrodes such as carbon or steel,<sup>5</sup> implying the need for catalysts (commonly expensive Pt).<sup>6</sup> Therefore, although being an environment-friendly technology, the application of MFCs in large scale is still limited by its low efficiency and high cost. Considerable efforts had been made on the improvement of performance based on unit cost by optimizing various operational parameters, such as electrode material, electrode surface area

and spacing, temperature, substrate flow, and others.<sup>7–12</sup> The inexpensive non-noble metal materials such as transition metal porphyrines and phthalocyanines,<sup>13</sup> Fe<sup>3+</sup> made with ferric sulfate,<sup>14</sup> metal oxides<sup>15</sup> have also been proposed as alternatives to Pt. However, their potentially secondary pollution caused by leaching of the transition metal ions out of the catalyst can not be avoided completely. Recently, great attention has been paid to using harmless and inexpensive carbon materials as anode or cathodic ORR catalyst.<sup>16–24</sup> Their common objectives were to establish more ORR catalyst sites and proton transfer chains by the increase of specific surface area. However, most researchers overlooked the hydrophobic gas diffusion channels in the catalyst layer (CL) design. Zhang et al. tested an air-cathode where polytetrafluoroethylene (PTFE) bonded activated carbon (AC) were pressed as CL, and reported an excellent performance in single-chambered MFC compared to Pt catalyst.<sup>19</sup> Very recently, their group reported a direct pressed AC-PTFE air cathode.<sup>24</sup> Wang et al. proposed a 3-D concept in their carbon nanotube (CNT) modified air-cathode, however, with a very complicated fabrication process.<sup>23</sup> In our previous work, the rolling method was introduced to make a novel activated carbon air-cathode (ACAC) containing large amounts

Received: September 6, 2012

Revised: November 2, 2012

Accepted: November 14, 2012

Published: November 14, 2012

of three phase interfaces (TPIs) in the CL, with a maximum power density of  $802 \text{ mW}\cdot\text{m}^{-2}$ .<sup>25</sup> It was further improved to  $1086 \text{ mW}\cdot\text{m}^{-2}$  by avoidance of sintering on CL.<sup>26</sup> However, the catalysis kinetics and pore analysis of this ACAC had not yet been identified. In this work, commercial AC powders with different specific areas as well as non-AC powder were used as catalyst in CLs along with the same gas diffusion layer (GDL). The catalysis behavior was investigated here by integrating catalysis kinetics with the microstructure analysis and MFC performance achieved.

## EXPERIMENTAL SECTION

**Air-Cathodes Fabrication.** The GDLs of the air-cathode used in this study were prepared in parallel by rolling carbon black (Jinqiushi Chemical Co. Ltd., Tianjin, China) and PTFE (60 wt %, Horizon, Shanghai, China) with a mass ratio of 3:7 as previously described.<sup>25</sup> Six identical GDL films were rolled onto stainless steel meshes ( $4 \text{ cm} \times 4 \text{ cm}$ ) and then sintered at  $340^\circ\text{C}$  for 25 min. Three carbon powders, including carbon black XC-72 (Horizon, Shanghai, China), plain AC (designated AC1#, Kewei Co. Ltd., Tianjin, China), and ultracapacitor AC (designated AC2#, Xinsen Carbon Co. Ltd., Fujian, China), were respectively utilized with PTFE binder (14 wt % content) to make different CLs.<sup>25</sup> Although both of them are ACs, AC2# has much larger specific surface area than that of AC1# (see Table 2). Because the performance of ACAC can be improved when the CL is not sintered,<sup>26</sup> the heating processes on CLs were avoided in all samples. Here “sintered” means “heated at  $340^\circ\text{C}$  for 25 min” in the procedure reported by Dong et al.<sup>25</sup> Since CLs were rolled on the opposite side of GDLs to achieve final air-cathodes (sampled as CAC, ACAC1#, and ACAC2# in turn), CL films were simultaneously prepared for the structure analysis. All the carbon powders used in this study had been pretreated to eliminate the ash.

**Electrochemical Measurements.** The electron transfer numbers ( $n$ ) of ORR catalyzed by the three carbon powders were estimated by the rotating disk electrode (RDE, AUT-RDE, Metrohm Ltd., Switzerland),<sup>27</sup> with Pt/C powder (10% HPPt on Vulkan XC-72, HeSen, Shanghai, China) as the control. A glassy carbon (GC) disk electrode with a diameter of 4 mm was assembled on RDE, where different catalysts were uniformly coated. Prior to use, the bare GC electrode was first polished with  $\text{Al}_2\text{O}_3$  powders (particle sizes of 0.05 mm). The polished electrode was successively cleaned with ethanol and distilled water in an ultrasonic bath, with 10 min for each step. The ink containing each sample of  $4.5 \text{ mg}\cdot\text{mL}^{-1}$  was prepared in a diluted Nafion solution ( $100 \mu\text{L}$ , 5%, diluted by 2-propanol and deionized water into 1.1 mL) and ultrasonically mixed to form the uniform ink. A  $4.5 \mu\text{L}$  aliquot of ink was then pipetted onto the GC surface to form a thin catalyst layer. After air-drying completely, the RDE was equipped in a three-electrode electrochemical cell and connected to a potentiostat (Autolab PGSTAT302N, Metrohm Ltd., Switzerland) for measurements. The linear scanning voltammetry (LSV) tests were performed at room temperature in 0.1 M potassium chloride solution with the RDE as the working electrode, a platinum electrode as the counter electrode, and Ag/AgCl (saturated KCl, 0.197 V versus SHE) as the reference electrode. Before each test, the solution was bubbled with  $\text{O}_2$  (99.999%) for 20 min to obtain the  $\text{O}_2$ -saturated environment. During the measurement,  $\text{O}_2$  was still supplied to the headspace of the electrolyte to maintain the oxygen saturation. Current values were recorded in respective proper potential window with a scan rate of  $1 \text{ mV}\cdot\text{s}^{-1}$ .

Tafel plots were conducted in a self-assembled three electrode cell filled with 50 mM phosphate buffer solution (PBS) using a potentiostat (CHI660D, Chenhua Instrument Co., China) as previously described.<sup>5</sup> Fresh CAC, ACAC1#, and ACAC2# were immersed in PBS for 3 days before equipped as the working electrodes ( $7 \text{ cm}^2$ ). A platinum sheet of  $1 \text{ cm}^2$  was sealed on the anodic side as the counter electrode. The reference electrode of Ag/AgCl (saturated KCl, 0.197 V versus standard hydrogen electrode, SHE) was spaced 0.5 cm from the working electrode. The plots of logarithm current density ( $\lg j$ ,  $\text{A}\cdot\text{cm}^{-2}$ ) versus overpotential ( $\eta$ , V) were recorded by sweeping the overpotential from 0 to 100 mV at  $1 \text{ mV}\cdot\text{s}^{-1}$ .

The deformation Tafel eq 1 can not only be used to obtain the value of  $j_0$  but also to estimate the electron transfer number  $n$  during the ORR, given as follows:

$$\lg j = \lg j_0 + (\beta n F / 2.303 RT) \eta \quad (1)$$

Corresponding to the Tafel plot, the slope is  $\beta F / 2.303 RT$  and the  $y$ -axis intercept is the  $\lg j_0$ . The resulting symmetry factor  $\beta$  is pH-dependent and typically less than 0.5 in the cathodic ORR.

All these electrochemical experiments were performed at ambient temperature ( $25 \pm 1^\circ\text{C}$ ).

**Pore Characterization.** The specific surface areas of XC-72, AC1#, and AC2# were identified using TriStar II 3020 (Micromeritics, ASAP2010, USA) and multipoint Brunauer–Emmett–Teller (BET) measurement through nitrogen adsorption at 77 K. Pore volume and pore size distribution of carbon powder were determined using the Barrett–Joyner–Halenda (BJH) model, based on the Kelvin equation and corrected for multilayer adsorption.<sup>28</sup> The porous structure of the CL was characterized with a mercury porosimeter (Autopore IV, Micromeritics). The pressure was from  $1.38 \times 10^3$  to  $4.13 \times 10^7 \text{ Pa}$  and the mercury contact angle was  $140^\circ$ . The pore size distribution and average pore size were determined from the mercury intrusion by the applied pressure based on capillary law. The surface morphology image of carbon powder and the corresponding CL were observed by scanning electron microscope (SEM, QUANTA 200, FEI Co., USA).

**MFC Tests.** A single-chambered cubic-shaped MFC reactor was constructed as previously described.<sup>25</sup> The total volume of each reactor was 28 mL. Heat-treated carbon mesh ( $450^\circ\text{C}$  for 30 min) was used as the anode in all of the experiments<sup>12</sup> while air-cathodes were the CAC, ACAC1#, and ACAC2#. Both the anode and cathode had the projected surface area of  $7 \text{ cm}^2$ . Reactors were operated in fed-batch mode in a constant temperature room ( $30 \pm 1^\circ\text{C}$ ) and refreshed when voltages reduced below 30 mV, forming one cycle ( $\sim 2$  days). All the tests were performed in triplicate.

## RESULTS

**Catalysis Kinetics on ORR.** The catalysis kinetics on ORR can be evaluated according to the electron transfer number ( $n$ ) which is usually calculated according to Koutecky–Levich plot.<sup>29</sup> RDE-based LSVs recorded at different rotating speeds and K–L plots for XC-72, AC1#, AC2#, and Pt/C catalysts are given in the Supporting Information (Figure 1S). The calculated  $n$  values were 2.1, 2.6, and 3.0 for XC-72, AC1#, and AC2# respectively, compared to the value of 3.9 obtained with Pt/C (same with the result reported by Cheng et al.<sup>27</sup>). This indicated that oxygen was mainly reduced to  $\text{H}_2\text{O}_2$  when

catalyzed by XC-72, while the proportion of O<sub>2</sub> which was completely reduced to H<sub>2</sub>O was increased on the surface of AC1# and AC2# ink. In the view of catalysis kinetics, Pt was the best to reduce the active energy of ORR needed than carbon materials. The excellent ORR performance of ACAC compared to traditional Pt/C air-cathode did not depend on the catalytic activity of AC powder itself.

Exchange current density ( $j_0$ ) was used to evaluate the ORR performance on different rolling CLs.<sup>30</sup> The fitting results according to the Tafel plots (Supporting Information Figure 2S) are listed in Table 1 where  $j_0$  of brushed Pt/C air-cathode

**Table 1. Linear Fit Equations, Exchange Current Densities, and Electron Transfer Number Calculated from the Linear Region of the Tafel Plots**

air cathodes	fit linear equation	( $R^2$ )	$10^{-4}j_0$ (A·cm <sup>-2</sup> )	electron transfer number
CAC	$y = -4.12010 + 1.31434x$	(0.99711)	0.76	2.2
ACAC1#	$y = -3.84590 + 4.35063x$	(0.99901)	1.43	3.2
ACAC2#	$y = -3.80233 + 4.11246x$	(0.99873)	1.58	3.5
brushed Pt/C	$y = -4.0508 + 3.23459x$	(0.99652)	0.89	2.4

with Nafion binder was also provided as the control. Approximate  $j_0$  values were achieved from ACAC1# ( $1.58 \times 10^{-4}$  A·cm<sup>-2</sup>) and ACAC2# ( $1.43 \times 10^{-4}$  A·cm<sup>-2</sup>), with values of 78% and 61% higher than that of brushed Pt/C air-cathode ( $0.89 \times 10^{-4}$  A·cm<sup>-2</sup>), predicting a better ORR performance with ACACs than that with brushed Pt/C air-cathode near the equilibrium potential. The  $j_0$  of CAC was 52% lower than that of ACAC1#, indicating a poorer catalytic activity of CAC on ORR. In eq 1, we assumed 0.2 in our ORR conditions to calculate  $n$  values (Table 1). The  $n$  values achieved from the rolling CAC and ACACs were all increased compared to those values obtained from RDE measurements except the brushed Pt/C air-cathode.

**Porous Structure of the Carbon Powders and CLs.** N<sub>2</sub> adsorption technique, a direct measure for the porous properties and structure on pore size distribution in the micro- (<2 nm), meso- (2–50 nm), and macroporosity ranges (>50 nm),<sup>31</sup> was conducted to determine the amount of gas adsorbed on the three carbon materials. The adsorption and desorption isotherms for the AC and non-AC powders (Supporting Information) belonged to type IV according to IUPAC.<sup>32</sup> These isotherms implied that the three carbon powders were all amorphous carbon with random pore distribution and interconnected pore system. The initial part of the isotherm was attributed to unrestricted monolayer–multilayer adsorption, from which the micropore area/volume were obtained below  $P/P_0 < 0.1$  and listed in Table 2. The largest micropore area/volume was AC2# ( $535 \text{ m}^2\cdot\text{g}^{-1}$ ,  $0.23 \text{ cm}^3\cdot\text{g}^{-1}$ ), followed by AC1# ( $269 \text{ m}^2\cdot\text{g}^{-1}$ ,  $0.12 \text{ cm}^3\cdot\text{g}^{-1}$ ) and XC-72 ( $96 \text{ m}^2\cdot\text{g}^{-1}$ ,  $0.04 \text{ cm}^3\cdot\text{g}^{-1}$ ) corresponding to the plots in Supporting Information Figure 3S. The hysteresis loops of non-AC and AC powders at higher  $P/P_0$  usually associated with capillary condensation in mesopore structures were type H3 and type H4, respectively.<sup>32,33</sup> Steeper shape in type H3 than in type H4 represented more mesopore and probably macropore adsorption, which led to a significant larger average pore size of non-AC (5.6 nm from BET and 12.6 nm from BJH) than those

**Table 2. Porous Structural Characteristics of Different Carbon Powders and CLs**

	carbon powders		
	XC-72	AC1#	AC2#
specific surface area (BET), $\text{m}^2\cdot\text{g}^{-1}$	268	576	1701
micropore area, $\text{m}^2\cdot\text{g}^{-1}$	96	269	535
mesopore area, $\text{m}^2\cdot\text{g}^{-1}$	172	307	1165
total volume, $\text{cm}^3\cdot\text{g}^{-1}$	0.60	0.45	1.0
micropore volume, $\text{cm}^3\cdot\text{g}^{-1}$	0.04	0.12	0.23
$A_{\text{Mic}}/A_{\text{Tot}}$ %	36	47	31
adsorption average pore width ( $4 \text{ V/A}$ by BET), nm	5.6	2.8	2.5
BJH desorption average pore width, nm ( $4 \text{ V/A}$ ), nm	12.6	4.0	3.5
CLs			
	CL with XC-72	CL with AC1#	CL with AC2#
total pore area, $\text{m}^2\cdot\text{g}^{-1}$	0.102	0.03	0.045
total intrusion volume, $\text{mL}\cdot\text{g}^{-1}$	0.47	0.15	0.25
average pore diameter, $\mu\text{m}$ ( $4 \text{ V/A}$ )	18.3	20.5	22.4
porosity, %	15.35	9.81	9.75

of AC1# (2.8 nm from BET and 4.0 nm from BJH) and AC2# (2.5 nm from BET and 3.5 nm from BJH) (Table 2). The mesopore area based on the BJH calculation showed AC2# ( $1165 \text{ m}^2\cdot\text{g}^{-1}$ ) was the largest one, followed by AC1# ( $307 \text{ m}^2\cdot\text{g}^{-1}$ ) and XC-72 ( $172 \text{ m}^2\cdot\text{g}^{-1}$ ). The pore size distribution was plotted according to the adsorption branch in order to avoid the artificial peak in desorption branch caused by the tensile strength effect in “ink bottle” pore<sup>34</sup> (Figure 1a). Near-vertical climbing shape in the curves of AC1# and AC2# was observed during the pore size less than 2 nm while the curve of XC-72 showed a relatively mild climb over the micropore area/volume range. In addition, the pore size of XC-72 distributing in mesoporosity and macroporosity range was wider than that of ACs, corresponding to the particular ascending straight line segment (30–90 nm) in Figure 1b. The proportion of micropore area in the total area was also compared and the highest value was achieved from AC1# (47%), followed by XC-72 (36%) and AC2# (31%). The random pore size distributions and interconnected pore systems in the three carbon powders can be observed from SEM images at magnification of 20K (Figure 2).

Dissimilarly, pores in the rolling CLs were formed by the aggregates of carbon particles with PTFE binder, and mainly ranged in mesoporosity and macroporosity which can be measured by the mercury intrusion measurement. The pore sizes of all the CLs exhibited bimodal distribution (Figure 3a), including an intense distribution at  $6 \mu\text{m}$  and a faint one at  $30 \mu\text{m}$  within macropore range as reported by Watanabe et al.<sup>35</sup> It is shown in Table 2 that the difference in micropore and mesopore distribution among XC-72 and ACs nearly had no effect on the pore size distribution of corresponding CLs since the dominated pores were macropores. The largest total pore volume expressed by the total mercury intrusion volume was obtained from the CL of XC-72 ( $0.47 \text{ mL}\cdot\text{g}^{-1}$ ), which may contain the open mesopore and macropore volumes of the carbon particles in CL (Figure 4). A lower volume were the CL of AC2# ( $0.25 \text{ mL}\cdot\text{g}^{-1}$ ), followed by the CL of AC1# ( $0.15 \text{ mL}\cdot\text{g}^{-1}$ ) (Table 2, Figure 3b). The SEM images at magnification of 10K displayed the difference in the surface

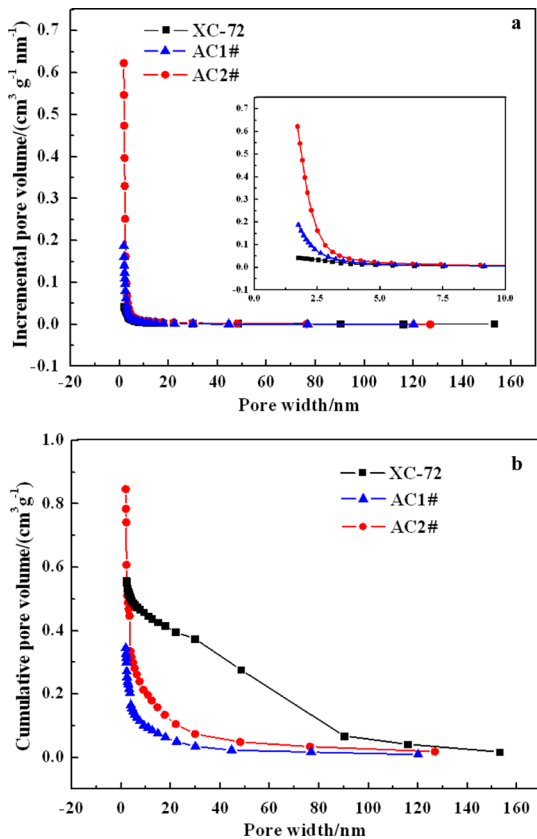


**Figure 1.** Pore size distributions (a) and cumulative pore volume (b) of the XC-72, AC1#, and AC2#. Inset figure in (a): detail of the pore size distribution over the range of 0–10 nm.

morphology of the three CLs (Figure 4). PTFE fibers in the CLs of AC1# and AC2# appeared more brawny and tight than those in the CL of XC-72 where PTFE can not be seen clearly.

#### Performance of MFCs with Different Carbon Powders.

The performance of CAC, ACAC1#, and ACAC2# in MFCs was compared to investigate the effect of pore structure in the carbon powder on the ORR performance. Similar open circuit voltages (OCVs) were observed in polarization plots of MFCs with ACAC1# ( $0.670 \pm 0.004$  V) and ACAC2# ( $0.692 \pm 0.004$  V), giving values 25% and 29% higher than that of CAC (Figure 5a). The activation polarization loss was not obvious in MFCs using ACACs, but it can be clearly seen in the MFC using CAC, especially when the current density was below  $0.8 \text{ A m}^{-2}$ . Although the MFC using ACAC2# achieved the highest OCV, the maximum power density of  $1355 \pm 26 \text{ mW m}^{-2}$  was given by the MFC using ACAC1#, which was 25% higher than that using ACAC2# ( $1086 \pm 8 \text{ mW m}^{-2}$ ) (Figure 5a). However, they were both much larger than  $464 \pm 11 \text{ mW m}^{-2}$  of MFC using CAC. The differences in the power densities and voltages resulted from the cathodes according to the electrode potential curves (Figure 5b).

## DISCUSSION

It had been proved that excellent and stable power output can be achieved from single-chambered MFC using rolling AC-PTFE air-cathode in our previous works.<sup>25</sup> The increase of 35% in the maximum power density was achieved by avoidance of sintering on CL.<sup>26</sup> However, the specific functions of AC powder and its catalysis mechanism have not yet been described clearly. In this work, we tried to explain this based

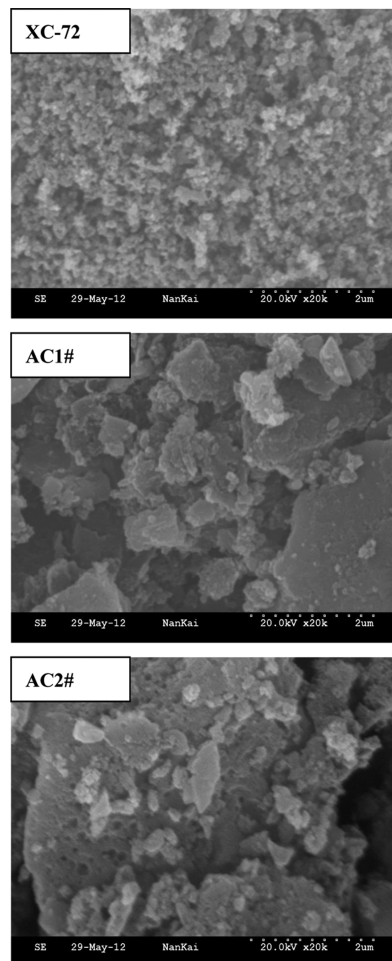


**Figure 2.** SEM images of the XC-72, AC1#, and AC2#.

on the pore structure and catalysis kinetics of the carbon powder itself and corresponding CL. By comparing the electron transfer number of ORR from RDE measurements and Tafel plots, increased values from 5% to 23% were found after the carbon powders were made into CLs by rolling method with PTFE, while it reversely decreased by 38% after the Pt/C powder was made into CL by brushing method with Nafion. In addition, remarkable catalytic ability of Pt to ORR was no longer observed in MFC since the higher power output was obtained from ACACs than that from brushing Pt/C air-cathode.<sup>25</sup> They gave us a notice that structure optimization of CL is more convenient and effective than exploring a novel catalyst with higher catalysis kinetics to the ORR in MFCs. Although oxygen deficiency in the RDE measurements can be ignored due to the continuous oxygen aeration, it was a dominant limitation of ORR performance in air-cathode of MFCs. Therefore, the porous structure of rolling CL for gas transfer by using hydrophobic PTFE instead of hydrophilic Nafion compensated the relative low catalysis kinetics of carbon powders on ORR via TPIs establishment. For porous catalyst especially, large amounts of TPIs in inner pores can be flooded by hydrophilic sulfonic groups in Nafion. Whether being activated or not, the pore sizes of these rolling CLs all concentrated at 6 μm (Table 2 and Figure 3a), indicating that these 6-μm macropores should be formed by mutual adhesion of carbon particles and PTFE fibers during rolling process and worked as the main stem of gas transfer.

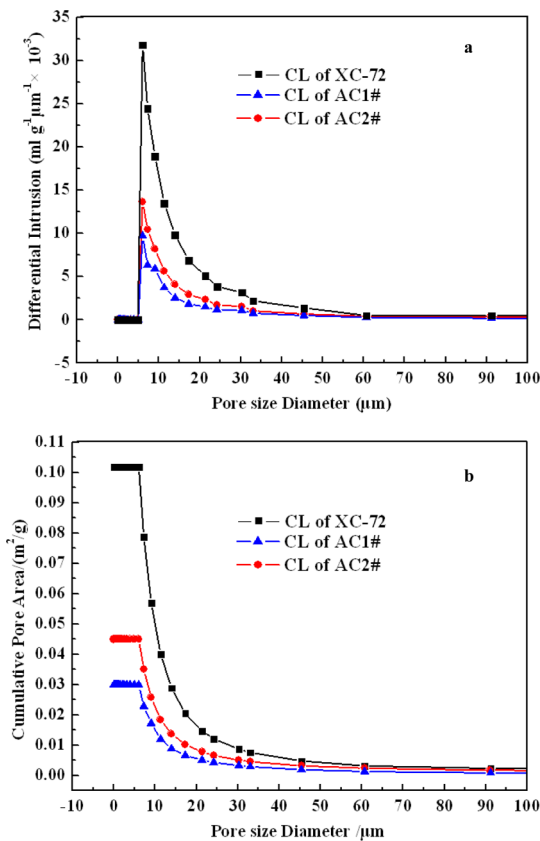


**Figure 3.** The pore size distribution (a) and the cumulative pore area versus the pore size diameter (b) of the CLs made from XC-72, AC1#, and AC2#.

However, the hydrophobic binder and rolling method were not the only factors that affected the performance since ORR *n* value of CAC was 31–37% lower than ACACs and the maximum power density of MFCs with CAC was 57–66% lower than those with ACACs. It should be attributed to the difference in the pore structure between XC-72 (non-AC) and ACs. According to the BET measurement, the specific surface areas of ACs were a factor of 1.15–5.35 larger than that of XC-72, because ACs had been additionally treated with steam at high temperature (800–1000 °C) during the production process, so that widespread interconnected porous structure especially micropores and mesopores existed in the ACs (Supporting Information Figure 4S). Most pores in AC1# and AC2# were uniformly distributed in microporosity, while wider pore distribution from mesoporosity to macroporosity was found in XC-72 based on BJH analysis. These micropores in ACs may provide additional ORR sites leading to a better ORR performance than that of XC-72. In other words, the TPI can be established on the surface of the micropores in addition to mesopores and macropores. The oxygen from the main stem of gas flow first diffused to the liquid film on the surface of macropores and mesopores, and then further diffused to the inner micropores (Supporting Information Figure 4S). Thus, to have abundant micropores in AC was another crucial factor for the excellent power output of air-cathode.

By comparing the catalysis kinetics (especially the ORR *n* value) of ACAC1# and ACAC2#, the additional specific surface area of ultracapacitor AC (AC2#) powder had little effect on the ORR performance (Table 1). The catalysis activity of ACs to ORR can be attributed to the additional reaction sites

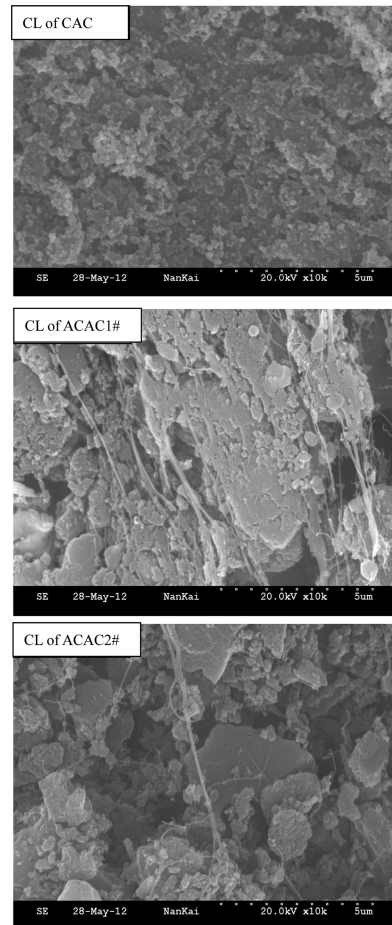


**Figure 4.** SEM images of the CL made from XC-72, AC1#, and AC2#, respectively, with PTFE binder.

provided by the abundant micropore structure (Table 2). As shown in Supporting Information Figure 5S, the *n* value of carbon powder was better linearly related with micropore area than mesopore area. For example, 2.7 times of increase in mesopore area of AC2# than AC1# did not result in a significant increase in *n* value (from 2.6 to 3.0), indicating that mesopores are less important than micropores for catalytic activity to ORR. When different carbon samples were rolled into CL, *R*<sup>2</sup> of both fittings decreased, illustrating other factors besides pore area were introduced.

Although the specific surface area of AC2# was two times larger than that of AC1#, the maximum power density of MFC using ACAC1# was reversely 25% higher than that using ACAC2#. Based on the weighing results that CL of AC1# contained 1 g of AC1# powder and CL of AC2# contained 0.7 g AC2#, the maximum power density of MFC using ACAC1# normalized to specific surface area ( $1.3 \times 10^{-3}$  mW·m<sup>-2</sup>) was 63% higher than that using ACAC2# ( $0.80 \times 10^{-3}$  mW·m<sup>-2</sup>) while both values were close to each other when the power density was calculated normalized to micropore area ( $3.5 \times 10^{-3}$  and  $2.0 \times 10^{-3}$  mW·m<sup>-2</sup> for ACAC1# and ACAC2#). This should be attributed to the 52% increase in the ratio of micropore area/total pore area of AC1# than that of AC2# (Table 2). In other words, dominant and uniform micropore distribution in AC powder has solid effect on improving the performance of ACAC in MFC. From this study, we found that the porous CL structure via hydrophobic binder and rolling

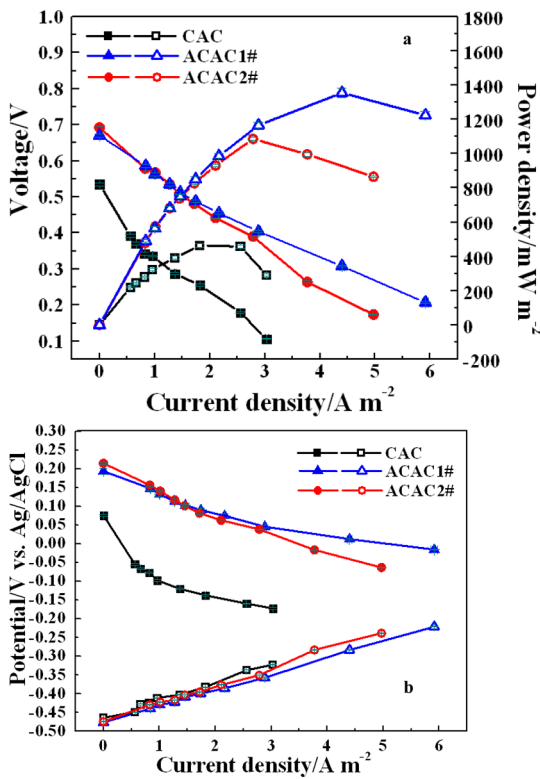


**Figure 5.** Polarization and power density curves (a) and electrode potentials (b) of MFCs using different carbon powders as air cathode catalyst. Standard deviations were calculated based on the average results of three samples in each case.

method and porous carbon powder with uniform micropore distribution were two crucial aspects to the excellent performance of ACAC. With a rough calculation, the cost of air-cathode can be substantially decreased from  $1400 \text{ \$}\cdot\text{m}^{-2}$  (Pt/C-Nafion-Carbon cloth) to  $30\text{--}60 \text{ \$}\cdot\text{m}^{-2}$  (ACAC). More efforts should be paid to the technology of pore distribution management in AC powder in the future.

## ASSOCIATED CONTENT

### Supporting Information

Additional figures as mentioned in the text. This information is available free of charge via the Internet at <http://pubs.acs.org/>.

## AUTHOR INFORMATION

### Corresponding Author

\*Phone: (86)22-23502756; fax: (86)22-23502756; E-mail: hongbingyu1130@sina.com (H.Y.); xinwang1@nankai.edu.cn (X.W.).

### Notes

The authors declare no competing financial interest.

## ACKNOWLEDGMENTS

This research work was supported by the National Science and Technology Support Project (2008BAC43B01) and National Natural Science Foundation of China (21107053 and 51208352). We appreciated the valuable discussion with Prof. Jun Chen of Nankai University, Dr. Tao Lei of Metrohm Autolab, Prof. Feng Zhao of Institute of Urban Environment (Chinese Academy of Sciences), and Dr. Guolong Zang of University of Science and Technology of China.

## NOMENCLATURE

MFCs	microbial fuel cells
GDL	gas diffusion layer
CL	catalyst layer
ORR	oxygen reduction reaction
TPI	three-phase interface
AC	activated carbon
PTFE	polytetrafluoroethylene
ACAC	activated carbon air-cathode
MPDs	maximum power densities
CE	Coulombic efficiency

## REFERENCES

- (1) Logan, B.; Cheng, S.; Watson, V.; Estadt, G. Graphite fiber brush anodes for increased power production in air-cathode microbial fuel cells. *Environ. Sci. Technol.* **2007**, *41* (9), 3341–3346.
- (2) Logan, B.; Rabaey, K. Conversion of wastes into bioelectricity and chemicals by using microbial electrochemical technologies. *Science* **2012**, *337*, 686–689.
- (3) Dewan, A.; Beyenal, H.; Lewandowski, Z. Scaling up Microbial Fuel Cells. *Environ. Sci. Technol.* **2008**, *42* (20), 7643–7648.
- (4) Wang, X.; Cai, Z.; Zhou, Q. X.; Zhang, Z. N.; Chen, C. H. Bioelectrochemical stimulation of petroleum hydrocarbon degradation in saline soil using U-tube microbial fuel cells. *Biotechnol. Bioeng.* **2012**, *109* (2), 426–433.
- (5) Dong, H.; Yu, H.; Wang, X.; Zhou, Q.; Sun, J. Carbon-supported Perovskite Oxides as Oxygen Reduction Reaction Catalyst in Single Chambered Microbial Fuel Cells. *J. Chem. Technol. Biotechnol.* **2012**, DOI: 10.1002/jctb.3893.
- (6) Zhao, F.; Slade, R. C. T.; Varcoe, J. R. Techniques for the study and development of microbial fuel cells: An electrochemical perspective. *Chem. Soc. Rev.* **2009**, *38* (7), 1926–1939.
- (7) Wen, Z.; Ci, S.; Zhang, F.; Feng, X.; Cui, S.; Mao, S.; Luo, S.; He, Z.; Chen, J. Nitrogen-Enriched Core-Shell Structured Fe/Fe3C-C Nanorods as Advanced Electrocatalysts for Oxygen Reduction Reaction. *Adv. Mater.* **2012**, *24* (11), 1399–1404.
- (8) Rabaey, K.; Clauwaert, P.; Aelterman, P.; Verstraete, W. Tubular microbial fuel cells for efficient electricity generation. *Environ. Sci. Technol.* **2005**, *39* (20), 8077–8082.
- (9) Wang, X.; Feng, Y. J.; Liu, J.; Shi, X. X.; Lee, H.; Li, N.; Ren, N. Q. Power generation using adjustable Nafion/PTFE mixed binders in air-cathode microbial fuel cells. *Biosens. Bioelectron.* **2010**, *26* (2), 946–948.
- (10) Liu, H.; Cheng, S. A.; Logan, B. E. Power generation in fed-batch microbial fuel cells as a function of ionic strength, temperature, and reactor configuration. *Environ. Sci. Technol.* **2005**, *39* (14), 5488–5493.
- (11) Li, F.; Sharma, Y.; Lei, Y.; Li, B.; Zhou, Q. Microbial Fuel Cells: The Effects of Configurations, Electrolyte Solutions, and Electrode Materials on Power Generation. *Appl. Biochem. Biotechnol.* **2010**, *160* (1), 168–181.
- (12) Wang, X.; Cheng, S. A.; Feng, Y. J.; Merrill, M. D.; Saito, T.; Logan, B. E. Use of Carbon Mesh Anodes and the Effect of Different Pretreatment Methods on Power Production in Microbial Fuel Cells. *Environ. Sci. Technol.* **2009**, *43* (17), 6870–6874.
- (13) Zhao, F.; Harnisch, F.; Schroder, U.; Scholz, F.; Bogdanoff, P.; Herrmann, I. Application of pyrolysed iron(II) phthalocyanine and CoTMPP based oxygen reduction catalysts as cathode materials in microbial fuel cells. *Electrochim. Commun.* **2005**, *7* (12), 1405–1410.
- (14) Park, D. H.; Zeikus, J. G. Improved fuel cell and electrode designs for producing electricity from microbial degradation. *Biotechnol. Bioeng.* **2003**, *81* (3), 348–355.
- (15) Roche, I.; Chainet, E.; Chatenet, M.; Vondrak, J. Carbon-supported manganese oxide nanoparticles as electrocatalysts for the Oxygen Reduction Reaction (ORR) in alkaline medium: Physical characterizations and ORR mechanism. *J. Phys. Chem. C* **2007**, *111* (3), 1434–1443.

- (16) Freguia, S.; Rabaey, K.; Yuan, Z.; Keller, J. Non-catalyzed cathodic oxygen reduction at graphite granules in microbial fuel cells. *Electrochim. Acta* **2007**, *53* (2), 598–603.
- (17) Duteanu, N.; Erable, B.; Kumar, S. M. S.; Ghangrekar, M. M.; Scott, K. Effect of chemically modified Vulcan XC-72R on the performance of air-breathing cathode in a single-chamber microbial fuel cell. *Bioresour. Technol.* **2010**, *101* (14), 5250–5255.
- (18) Jiang, D.; Li, B. Granular activated carbon single-chamber microbial fuel cells (GAC-SCMFCs): A design suitable for large-scale wastewater treatment processes. *Biochem. Eng. J.* **2009**, *47* (1–3), 31–37.
- (19) Zhang, F.; Cheng, S. A.; Pant, D.; Van Bogaert, G.; Logan, B. E. Power generation using an activated carbon and metal mesh cathode in a microbial fuel cell. *Electrochim. Commun.* **2009**, *11* (11), 2177–2179.
- (20) Liu, X.-W.; Sun, X.-F.; Huang, Y.-X.; Sheng, G.-P.; Zhou, K.; Zeng, R. J.; Dong, F.; Wang, S.-G.; Xu, A.-W.; Tong, Z.-H.; Yu, H.-Q. Nano-structured manganese oxide as a cathodic catalyst for enhanced oxygen reduction in a microbial fuel cell fed with a synthetic wastewater. *Water Res.* **2010**, *44* (18), 5298–5305.
- (21) Ahmed, J.; Yuan, Y.; Zhou, L.; Kim, S. Carbon supported cobalt oxide nanoparticles-iron phthalocyanine as alternative cathode catalyst for oxygen reduction in microbial fuel cells. *J. Power Sources* **2012**, *208*, 170–175.
- (22) Chen, Y.; Lv, Z.; Xu, J.; Peng, D.; Liu, Y.; Chen, J.; Sun, X.; Feng, C.; Wei, C. Stainless steel mesh coated with MnO<sub>2</sub>/carbon nanotube and polymethylphenyl siloxane as low-cost and high-performance microbial fuel cell cathode materials. *J. Power Sources* **2012**, *201*, 136–141.
- (23) Wang, H.; Wu, Z.; Plaseied, A.; Jenkins, P.; Simpson, L.; Engrakul, C.; Ren, Z. Carbon nanotube modified air-cathodes for electricity production in microbial fuel cells. *J. Power Sources* **2011**, *196* (18), 7465–7469.
- (24) Wei, B.; Tokash, J. C.; Chen, G.; Hickner, M.; Logan, B. Development of low-cost activated carbon cathodes for use in air-cathode microbial fuel cells. *RSC Advance* **2012**, DOI: 10.1039/C2RA21572A.
- (25) Dong, H.; Yu, H.; Wang, X.; Zhou, Q.; Feng, J. A novel structure of scalable air-cathode without Nafion and Pt by rolling activated carbon and PTFE as catalyst layer in microbial fuel cells. *Water Res.* **2012**, *46*, 5777–5787.
- (26) Dong, H.; Yu, H.; Wang, X.; Feng, J. Enhanced Performance of Activated Carbon-PTFE Air-cathode by Avoidance of Sintering on Catalyst Layer in Microbial Fuel Cells. *Water Res.* **2012**, under review.
- (27) Cheng, F.; Shen, J.; Peng, B.; Pan, Y.; Tao, Z.; Chen, J. Rapid room-temperature synthesis of nanocrystalline spinels as oxygen reduction and evolution electrocatalysts. *Nat. Chem.* **2011**, *3* (1), 79–84.
- (28) Barret, E. P.; Joyner, L. G.; Halenda, P. H. *J. Am. Chem. Soc.* **1951**, *73*, 373.
- (29) Cheng, F. Y.; Shen, J.; Ji, W. Q.; Tao, Z. L.; Chen, J. Selective Synthesis of Manganese Oxide Nanostructures for Electrocatalytic Oxygen Reduction. *ACS Appl. Mater. Interfaces* **2009**, *1* (2), 460–466.
- (30) Hamann, C. H.; Hamnett, A.; Vielstich, W. *Electrochemistry*; Wiley, 2008.
- (31) Rouquerol, F.; Rouquerol, J.; Sing, K. S. W. *Adsorption by Powders and Porous Solids*; Academic Press: London, 1999.
- (32) Sing, K. S. W. Reporting physisorption data for gas/solid systems with special reference to the determination of surface area and porosity (Recommendations 1984). *Pure Appl. Chem.* **1985**, *57* (4), 603–619.
- (33) Groen, J. C.; Peffer, L. A. A.; Pérez-Ramírez, J. Pore size determination in modified micro- and mesoporous materials. Pitfalls and limitations in gas adsorption data analysis. *Microporous Mesoporous Mater.* **2003**, *60* (1–3), 1–17.
- (34) Gregg, S. J.; Olds, R. M.; Tyson, R. F. S. Third conference on industrial carbon and graphite. Academic Press: London and New York, 1970.
- (35) Watanabe, M.; Tomikawa, M.; Motoo, S. Experimental analysis of the reaction layer structure in a gas diffusion electrode. *J. Electroanal. Chem.* **1985**, *195*, 81–93.